

# EMMA: Generalizing Real-World Robot Manipulation via Generative Visual Transfer

Zhehao Dong<sup>1,2\*</sup>, Xiaofeng Wang<sup>1,3\*</sup>, Zheng Zhu<sup>1\*†</sup>, Yirui Wang<sup>3</sup>, Yang Wang<sup>1</sup>, Yukun Zhou<sup>1</sup>  
 Boyuan Wang<sup>1,4</sup>, Chaojun Ni<sup>1,2</sup>, Runqi Ouyang<sup>1,4</sup>, Wenkang Qin<sup>1</sup>, Xinze Chen<sup>1</sup>, Yun Ye<sup>1</sup>  
 Guan Huang<sup>1</sup>, Zhen Lu<sup>2</sup>, Yue Yang<sup>2</sup>

<sup>1</sup>GigaAI, <sup>2</sup>Peking University, <sup>3</sup>Tsinghua University, <sup>4</sup>CASIA  
 {zhengzhu}@ieee.org

Project page: <https://emma-gigaai.github.io>

arXiv:2509.22407v2 [cs.AI] 16 Mar 2026

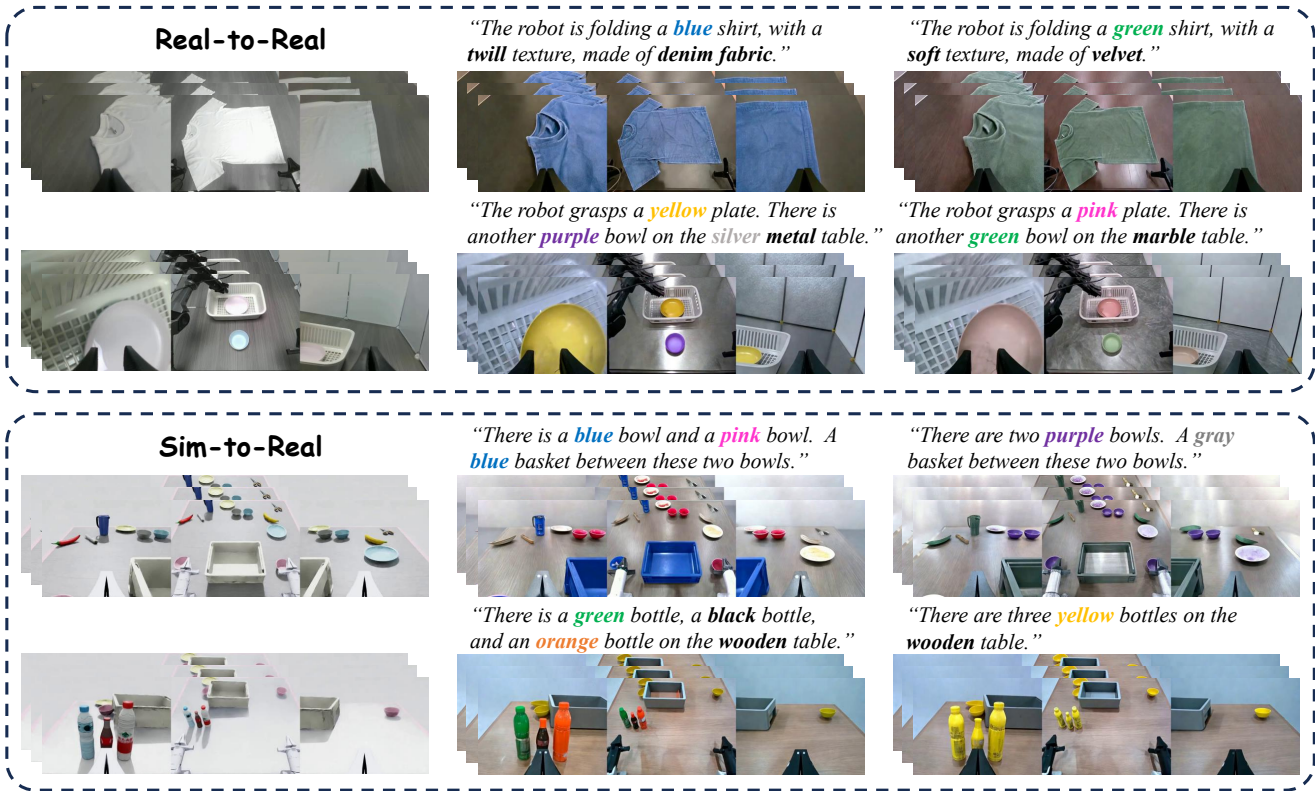


Figure 1. The first column shows data collected from real-world and simulated environments. The next two columns show diverse data generated by *DreamTransfer* from the first column. *DreamTransfer* demonstrates strong controllability in embodied manipulation video generation. It excels in text-guided appearance editing while preserving 3D structure and geometric plausibility, and supports both real-to-real and sim-to-real transfer. The complete prompts are provided in the supplementary material.

## Abstract

The generalization of vision-language-action (VLA) models heavily relies on diverse training data. However, acquiring large-scale data for robot manipulation across varied

object appearances is costly and labor-intensive. To address this limitation, we introduce *Embodied Manipulation Media Adaptation (EMMA)*, a framework for augmenting VLA policies that combines a generative data engine with an effective training pipeline. We introduce *DreamTransfer*, a diffusion Transformer-based architecture for generating multi-view consistent and geometrically plausible em-

\* Equal contribution.  
 † Corresponding author.

*bodied manipulation videos. DreamTransfer enables visual editing of robot videos through text, allowing for changes to the foreground, background, and lighting while preserving their 3D structure and geometric fidelity. We also utilize a hybrid training set of real and generated data and propose AdaMix to enhance the training process. AdaMix is a training strategy that adaptively weights samples according to policy performance to emphasize challenging samples. Comprehensive evaluations demonstrate that videos created by DreamTransfer yield substantial improvements over previous video generation models in multi-view consistency, geometric fidelity, and text-conditioning precision. We conduct extensive evaluations with a total of more than 1800 trials in both simulated and real-world robotic environments. In real-world robotic tasks with zero-shot visual settings, our framework achieves a relative performance increase of over 92% compared to training with real data alone, and improves by an additional 17% with AdaMix, demonstrating its efficacy in enhancing policy generalization.*

## 1. Introduction

Vision-language-action (VLA) models have demonstrated remarkable capabilities in enabling robots to perform complex manipulation tasks from natural language instructions and visual inputs [3, 5, 13, 20, 26, 42]. However, their success critically depends on large-scale, diverse training data. Collecting real-world robot manipulation data through human teleoperation is labor-intensive and expensive, severely limiting the scale and visual diversity of available datasets. While simulation offers a scalable alternative for generating annotated trajectories [15, 24, 32, 38], simulated environments often suffer from visual realism gaps and are constrained by limited asset diversity. As a result, VLA policies trained on simulated data frequently underperform when deployed in the real world.

Recently, diffusion models [28, 40, 49, 56, 65] have emerged as a promising method for generating realistic and diverse videos. Several works have explored using diffusion models to generate vision-action data for policy training. Cosmos-Transfer1 [41] generates videos conditioned on semantic segmentation and depth, improving realism for sim-to-real transfer. RoboEngine [58] provides a flexible toolkit for generating diverse robot interaction scenes by combining background generation with accurate robot segmentation. RoboTransfer [34] further improves multi-view consistency by explicitly modeling 3D geometry using depth maps and surface normals, allowing controllable edits.

Despite these advances, two key challenges remain. First, most methods [41, 58] generate videos from a single view, without ensuring consistency across viewpoints. This limits their usefulness for downstream robot tasks that

rely on multi-camera inputs. RoboTransfer takes a step toward multi-view consistency, but it relies on image-based conditioning and lacks the flexibility to edit manipulation videos via text. Second, existing works treat generated data as a static augmentation, without considering how to use it effectively during training.

In this work, we propose **Embodied Manipulation Media Adaptation (EMMA)**, a VLA policy enhancement framework that integrates two core components: *DreamTransfer* and *AdaMix*. *DreamTransfer* is a diffusion Transformer (DiT)-based framework for generating multi-view consistent, geometrically plausible embodied manipulation videos. It jointly models appearance and geometry across multiple camera views, ensuring spatial and temporal coherence. *DreamTransfer* supports text-guided visual transfer: users can edit the foreground objects, background, and lighting conditions of real or simulated demonstrations through natural language, while preserving the underlying 3D structure and geometric plausibility of the scene. As illustrated in Figure 1, *DreamTransfer* enables realistic and controllable video generation for both real-to-real and sim-to-real transfer scenarios, making it a powerful tool for scalable policy training. To improve policy learning, we further propose *AdaMix*, a hard-sample-aware training strategy. We propose three metrics to evaluate the quality of predicted trajectories from the VLA policy and use the performance score to drive an adaptive sampling mechanism. By iteratively refining the training distribution toward challenging cases, our method improves robustness and generalization.

We evaluate on a variety of robotic manipulation tasks in both video generation quality and real-world robot deployment, including Fold Clothes, Clean Desk, and Throw Bottle. These tasks span a wide range of challenges involving both rigid and deformable objects, short-horizon and long-horizon action sequences, and diverse skills such as grasping, pushing, placing, and draping. Compared to the state-of-the-art transfer model, *DreamTransfer* improves multi-view consistency by 42% and depth consistency by 24%, demonstrating superior cross-view coherence and geometric fidelity. In real-world robotic manipulation tasks involving zero-shot visual appearances, our method achieves over a 92% relative improvement in task success rate compared to training on real data alone, with an additional 17% gain when integrated with *AdaMix*.

In summary, our contributions are:

- We propose *EMMA*, a VLA policy enhancement framework that integrates a generative data engine with an effective training strategy. The data engine generates diverse, multi-view consistent robot manipulation videos for both rigid and deformable objects, while adaptive sample weighting improves VLA policy generalization.
- We propose *DreamTransfer*, a DiT-based model that generates multi-view consistent, geometrically plausible ma-

manipulation videos and supports text-guided editing of foreground, background, and lighting conditions. We further introduce *AdaMix*, a hard-sample-aware training strategy that identifies challenging trajectories and adaptively reweights them during training.

- *EMMA* demonstrates strong performance in video generation and real-world robotic deployment. Compared to the state-of-the-art model, *DreamTransfer* achieves a 42% gain in multi-view consistency and a 24% gain in depth consistency, measured relatively. In zero-shot visual settings, our method achieves over a 92% performance gain compared to real-data training, with *AdaMix* providing an additional 17% improvement and enhancing cross-domain visual generalization.

## 2. Related work

### 2.1. Visual Generalizable Imitation Learning

Imitation learning enables visuomotor policies to learn from human demonstrations, providing an effective pathway for robotic manipulation [11, 22, 31]. Recently, VLA models have significantly improved generalization by integrating semantic understanding into action generation [5, 26]. Early systems like CLIPort [46] established the foundation for vision-conditioned control, while subsequent works enhanced capabilities through chain-of-thought reasoning [64]. Recent advances include domain specialization [60], occlusion handling [53], and safety-aware execution [61]. Models like OpenVLA and EF-VLA [18] further improve performance through dual visual encoders or preserved semantic alignment, while self-correcting frameworks [29] enable recovery from failures in cluttered environments. However, VLA models perform poorly under limited real-world demonstrations and require large-scale and diverse data to generalize across objects and environments.

Collecting data across diverse objects and environments is expensive and time-intensive [12, 25]. This gap motivates using generated data as a scalable way to enrich visual diversity, provided that the generated content maintains geometric plausibility and spatial consistency.

### 2.2. Generative Models for Embodied Data

To improve generalization in VLA models, various generative approaches have been proposed to generate diverse robot data at low cost [7, 23, 33, 50, 59]. While traditional data augmentation techniques remain effective for in-domain generalization [11], they often struggle under significant visual distribution shifts. In contrast, generative models offer stronger cross-domain adaptation potential [48], yet many methods rely on additional inputs such as object masks or scene-specific annotations [10, 37, 51]. Furthermore, techniques based on inpainting or scene completion can exhibit instability across varied environments,

frequently requiring per-scene hyperparameter tuning to ensure reliable generation [57, 67]. Real-to-sim-to-real methods like RoboSplat [54] and ReBot [14] rely on simulators and are largely limited to rigid-body interactions, with some such as RoboGSim [30] requiring costly 3D reconstruction. Recent advances in diffusion models [4, 16, 17, 47] and video diffusion transformers [35, 56] have enabled high-fidelity generation of embodied manipulation videos. Our goal is to generate multi-view consistent embodied manipulation videos that can be flexibly edited via text. However, existing video generation models do not support such text-driven control over scene appearance while preserving cross-view consistency. Cosmos-Transfer1 [41] uses semantic segmentation and depth maps to generate realistic scenes. RoboDreamer [66] enables prompt-guided trajectory generation but may sacrifice geometric accuracy. RoboTransfer [34] improves multi-view consistency using depth and surface normals, but relies on image inputs and does not support text-based editing of manipulation videos.

## 3. Method

### 3.1. Framework Overview

We propose *EMMA*, a VLA policy enhancement framework that integrates two core components: *DreamTransfer* and *AdaMix*. As illustrated in Figure 2, *DreamTransfer* functions as a generative data engine for training VLA, capable of generating multi-view consistent, geometrically plausible robot manipulation videos from both real and simulated inputs. The framework supports fine-grained text-guided editing of visual attributes such as foreground objects, background scenes, and lighting, while preserving the underlying 3D geometry and action dynamics.

The pipeline begins with real or simulated demonstration videos, which are processed by *DreamTransfer* that generates robot manipulation videos across multiple camera views. The model ensures spatial and temporal coherence by jointly modeling multi-view appearance and geometry, which also effectively bridges the visual gaps between simulation and the real world. The generated videos are subsequently filtered according to depth consistency, multi-view consistency, and text-video similarity metrics. To ensure training stability, we initialize the training process using only high-quality videos by setting the sampling probability of low-quality videos to zero. To further enhance policy generalization, we introduce *AdaMix*, a hard-sample-aware training strategy that dynamically adjusts the sampling weights based on their trajectory performance metric. By adaptively emphasizing challenging cases, *AdaMix* enhances policy generalization and improves performance on real-world environments. Our framework advances effective policy learning for embodied manipulation by combining high-fidelity video generation with the adaptive sample



Figure 2. Overview of the *EMMA* framework. First, *DreamTransfer* generates multi-view consistent videos by performing text-guided visual editing of the foreground, background, and lighting conditions, conditioned on depth and corresponding text prompts. The generated videos are then evaluated by a video quality filter. Low-quality videos are initially assigned zero sampling weight to stabilize early-stage training. The *AdaMix* module further adaptively reweights training samples based on trajectory quality metrics, up-weighting challenging samples to improve policy robustness and generalization.

selection of *AdaMix*.

We first introduce the *DreamTransfer* model in Section 3.2, followed by a presentation of the *AdaMix* training strategy in Section 3.3.

### 3.2. DreamTransfer

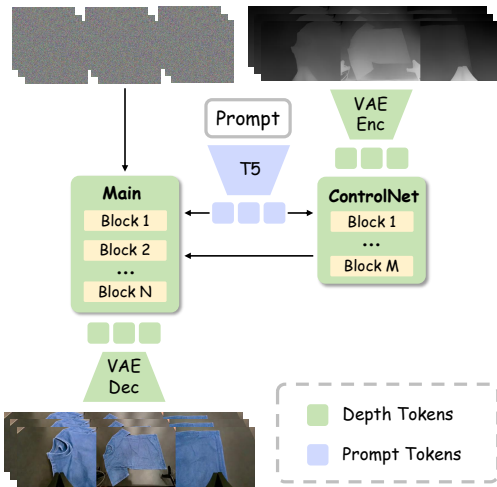


Figure 3. Overview of the *DreamTransfer* framework. Multi-view depth maps are concatenated along the width dimension. The main branch denoises latent video tokens, while a parallel ControlNet branch ensures geometric consistency by incorporating depth constraints.

The overall framework of *DreamTransfer* is illustrated in Figure 3. *DreamTransfer* features a dual-branch architecture, both built upon DiT-based framework [40, 41]. The main branch denoises latent video tokens, while the parallel ControlNet [62] branch enhances geometric consistency by

incorporating depth-based structural guidance.

*DreamTransfer* leverages multi-view in-context learning capabilities [19, 21, 34, 63] inherently present in pretrained diffusion models, which ensures spatial and temporal coherence across different camera viewpoints. First, multiple synchronized video depth from different viewpoints  $\{v^{(1)}, v^{(2)}, \dots, v^{(M)}\}$  are concatenated along the width dimension and encoded into a unified latent representation using a VAE encoder [27]:

$$d_{init} = \text{Enc}([v^{(1)}, v^{(2)}, \dots, v^{(M)}]). \quad (1)$$

In parallel, a pretrained T5 text encoder [44] converts text prompt into high-dimensional semantic embeddings. These textual features are fused with the visual latents via cross-attention, enabling fine-grained control over object appearance. The main branch then takes the noisy latent  $z_t$  at time step  $t$  together with the prompt features  $s$  and depth features  $d_t$ , to predict the denoised latent:

$$n = f_{\theta}(z_t, t, d_t, s), \quad (2)$$

where  $f_{\theta}$  denotes the diffusion transformer parameterized by  $\theta$ , and  $n$  represents the predicted denoised latent. Finally, the predicted denoised latent is decoded by the VAE decoder to reconstruct the output video, preserving the underlying 3D structure and faithfully reflects the prompt-specified appearance changes.

We construct a dataset of 50k multi-view video clips based on the Agibot World dataset [6], covering 36 diverse scenes. Each clip contains a length of 121 frames. *DreamTransfer* adopts a two-stage fine-tuning strategy that enables high-quality multi-view video generation with just 131 hours of training on four NVIDIA H20 GPUs. More training details of *DreamTransfer* are provided in Appendix A.

*DreamTransfer* generates 121-frame videos, which can be extended to long-horizon sequences via clip-wise generation and concatenation. For VLA policy training, each frame acts as an independent observation-action pair, providing sufficient data for effective learning.

### 3.3. AdaMix

After generating embodied manipulation data, how to use it effectively for training VLA policies remains an open challenge. Related ideas have been explored in other fields. For instance, Delphi [36] in autonomous driving improves generalization by focusing on failure cases, and POLARIS [1] in LLM-based reinforcement learning enhances training by filtering out overly simple questions. Inspired by these approaches, our work explores efficient training strategies tailored to downstream VLA policies.

We observe that, despite extensive fine-tuning on a large mixture of real-world demonstrations and generated data, VLA models still exhibit errors when evaluated on the training set. This observation reveals that uniform training paradigms fail to adequately address challenging, long-tail scenarios, even when those scenarios are included in the training data.

Building on this insight, we present *AdaMix*, a hard-sample-aware training strategy that dynamically reweights training data based on policy performance. Unlike uniform sampling schemes that treat all samples equally, *AdaMix* continuously identifies challenging scenarios, particularly those in the long-tail where policies typically struggle. By up-weighting these hard samples during training, *AdaMix* achieves improved generalization.

The *AdaMix* pipeline consists of three stages, as illustrated in right part of Figure 2. First, generated videos are evaluated by a video quality filter based on depth consistency, multi-view consistency, and text-video similarity. Samples failing to meet quality thresholds are assigned zero sampling weight, ensuring that only geometrically plausible and semantically faithful data are used for training. Then, the VLA model is initially trained using uniform sampling over real data and high-quality generated data. After the loss converges, we compute the following three predicted trajectory quality metrics on each training sample to identify challenging instances. These metrics are inspired by NVIDIA’s robotic policy benchmarking framework [55] and tailored to our setting.

**Action MSE.** We compute the Mean Squared Error (MSE) between the predicted action chunk  $\hat{a}_{i:t}$  and the corresponding ground-truth sequence  $a_{i:t}$  over a window of at most  $L$  frames:

$$r_i^{\text{MSE}} = -\frac{1}{L} \sum_{t=0}^{L-1} \|\hat{a}_{i+t} - a_{i+t}\|_2^2. \quad (3)$$

**Smoothness.** To encourage physically plausible actions,

we measure the second-order difference of joint angles to penalize abrupt joint actions:

$$r_i^{\text{Smooth}} = -\sum_j \left| \frac{a_{i+2,j} - 2a_{i+1,j} + a_{i,j}}{(\Delta t)^2} \right|, \quad (4)$$

where  $j$  indexes the joint dimension, and  $\Delta t$  represents the time interval between frames.

**Joint limitation.** We assign a binary indicator to ensure safety, setting

$$r_i^{\text{Limit}} = \begin{cases} 1, & \text{if all joint angles within thresholds,} \\ 0, & \text{otherwise.} \end{cases} \quad (5)$$

These scores are min-max normalized to  $\tilde{r}_i^{(\cdot)} \in [0, 1]$  and combined into a unified score per sample :

$$s_i = w_{\text{MSE}} \cdot \tilde{r}_i^{\text{MSE}} + w_{\text{Smooth}} \cdot \tilde{r}_i^{\text{Smooth}} + w_{\text{Limit}} \cdot \tilde{r}_i^{\text{Limit}}, \quad (6)$$

where  $w_{\text{MSE}} + w_{\text{Smooth}} + w_{\text{Limit}} = 1$  and each weight is non-negative. A higher  $s_i$  indicates better overall performance on the  $i$ -th sample. To find a suitable weighting scheme, we conducted an ablation study on the three metrics in Section 4.2.5. We find that these metrics exhibit comparable impact on performance. Therefore, we adopt equal weights for all three metrics.

During incremental training, sampling weights are updated as:

$$p(i) \propto \gamma + \lambda \cdot (1 - s_i), \quad (7)$$

where  $\gamma > 0$  ensures minimum support for all samples, and  $\lambda$  controls the emphasis on hard samples. We perform a quantitative analysis of the two key hyperparameters  $\gamma$  and  $\lambda$  in Section 4.2.4. The configuration  $\gamma = 1$ ,  $\lambda = 10$  achieves the best trade-off, and is adopted in this work.

By adaptively up-weighting samples where the policy performs poorly, the training distribution gradually shifts toward underperforming regions while preserving data diversity. Note that all evaluations and re-weighting are performed on the training data to prevent any potential leakage from validation data.

## 4. Experiments

In this section, we evaluate *EMMA* framework on both video generation and real-world robotic deployment. We conducted extensive experiments on diverse tasks such as Fold Clothes, Clean Desk, and Throw Bottle. The first task is real-to-real transfer, and the last two tasks are sim-to-real. These tasks cover a range of robotic tasks involving both rigid and deformable objects, long-horizon and short-horizon actions, and different manipulation skills such as grasping, pushing, and placing.

We first evaluate the quality of generated videos from *DreamTransfer* in Section 4.1. Then we use the generated

data to train downstream VLA policy model and deploy on real-world robot in Section 4.2. Finally, we conduct experiments in simulated environments in Section 4.3.

#### 4.1. Video Generation Quality

**Implementation details.** While general video generation models [4, 49, 56, 65] exhibit strong open-domain performance, they suffer from several limitations in embodied scenarios, specifically multi-view inconsistency and poor physical fidelity. We provide visualization results of general video generation models in Appendix D. Robotic task-specialized models such as Cosmos-Transfer1 [41] and RoboTransfer [34] leverage large-scale embodied data to achieve better kinematic plausibility, and we compare *DreamTransfer* with these specialized models. Both *DreamTransfer* and RoboTransfer natively support multi-view transfer, while Cosmos-Transfer1 is only designed for single-view generation. To ensure a fair comparison across all three models, we adopted model-adapted input and output processing strategies: for Cosmos-Transfer1, we processed each camera view independently and then concatenated the generated frames along the width dimension to form multi-view outputs; for *DreamTransfer* and RoboTransfer, we directly used the concatenated multi-view videos as input, enabling them to generate multi-view videos in a single inference pass. All generated videos are at a uniform resolution of  $1920 \times 480$  for fair evaluation, matching the platform’s hardware (three synchronized  $640 \times 480$  cameras) in real-world robot evaluations.

We collected 50 real demonstrations for `Fold Clothes` on the Agilex CobotMagic platform, and 20 simulated demonstrations for both `Clean Desk` and `Throw Bottle` in the NVIDIA Isaac Sim environment [39]. During demonstration collection, we ensured that the appearances of objects in the scene remained consistent, as shown in the first column of Figure 1 (rows 1, 3, and 4). For each model, we generated visually diverse demonstrations at a 1:1 ratio relative to the original data, resulting in 90 generated demonstrations per model (50 for `Fold Clothes` and 20 each for `Clean Desk` and `Throw Bottle`). We performed evaluations on these generated demonstrations for all models.

Our evaluation focuses on three key aspects: multi-view consistency, depth consistency, and text-to-video alignment. We assess multi-view consistency using the Matched Pixels (Mat.Pix.) metric, which is defined as the average number of pixel correspondences matched between the center camera view and the left/right wrist-mounted views across all frames. For depth consistency, we evaluate the fidelity of predicted depth against ground truth with three error metrics: Root Mean Squared Error (RMSE), Absolute Relative Error (Abs.Rel.), and Squared Relative Error (Sq.Rel.). Finally, text-to-video alignment is quantified by CLIP Simi-

larity (CLIPSim.) to measure how well the video matches the instruction. Input conditions are kept identical across models for fair comparison. The specific formulas for these metrics are provided in Appendix B.

**Results.** As shown in Table 1, *DreamTransfer* achieves the best performance across all metrics in most tasks and consistently outperforms both RoboTransfer and Cosmos-Transfer1 in multi-view consistency and geometric fidelity. On average, it improves pixel matching by 42% over the second-best model. This demonstrates that our multi-view conditioned generation produces highly consistent appearances across camera views. In depth consistency, *DreamTransfer* reduces Sq.Rel. to 0.54, a 24% improvement over Cosmos-Transfer1 and 58% over RoboTransfer. These gains are enabled by our explicit depth conditioning, which enforces cross-view structural coherence during video generation. Regarding text-video alignment, *DreamTransfer* scores 24.68 on average, surpassing both baselines and showing no loss in text semantic alignment. Visual comparisons are provided in Appendix D.

#### 4.2. Real-World Robot Evaluation

We conduct extensive experiments to evaluate our *EMMA* framework on real-world robotic tasks. We focus on three key questions: (1) Can co-training with generated data improve real-world policy performance and generalization to zero-shot object appearances? (2) How does the mixing ratio of real and generated data affect VLA policy performance? (3) Can *AdaMix*, our hard-sample-aware adaptive training strategy, further enhance real-world policy performance?

**Implementation details.** We adopt  $\pi_0$  [3] and  $\pi_{0.5}$  [20] as our base VLA policy model architecture without modifications and perform post-training on the pre-trained model. We evaluate our framework on three challenging real-world robotic tasks: `Fold Clothes`, `Clean Desk`, and `Throw Bottle`. Detailed descriptions of each task are provided in Appendix C.1.

We train policies on a mixed dataset  $D^\alpha$ , composed of real data  $D_R$  and generated data  $D_G$ . No.Aug. in Table 2 denotes training using real data only, where  $|D_R| = 50$  for `Fold Clothes` and  $|D_R| = 20$  for both `Clean Desk` and `Throw Bottle`. The subsequent two rows correspond to training with a 1:1 mixture of real data and data generated by Cosmos-Transfer1 [41] and *DreamTransfer*, as described in Section 4.1.  $|D_G| = |D_R| = 50$  for `Fold Clothes`, and  $|D_G| = |D_R| = 20$  for both `Clean Desk` and `Throw Bottle`. Unless otherwise specified, the training data settings described above are adopted for all experiments on each task. For each task, the real data is collected in a single environment with a fixed set of foreground objects. For instance, the real-world data for the `Fold Clothes` task only contains white shirt being folded. We

Table 1. Comparison of video generation quality on robot manipulation tasks. Best results are in **bold**. The result demonstrates that *DreamTransfer* achieves the best performance across all metrics.

Task	Model	Pix.Mat.(↑)	RMSE(↓)	Abs.Rel.(↓)	Sq.Rel.(↓)	CLIPSim.(↑)
Fold Clothes	RoboTransfer [34]	1736	3.97	0.50	2.13	24.63
	Cosmos-Transfer1 [41]	2210	2.78	0.36	1.14	25.02
	<i>DreamTransfer</i>	2604	2.50	0.32	0.97	24.54
Clean Desk	RoboTransfer [34]	3213	2.50	0.32	0.85	23.87
	Cosmos-Transfer1 [41]	2484	1.55	0.19	0.36	25.02
	<i>DreamTransfer</i>	4311	1.45	0.18	0.33	25.75
Throw Bottle	RoboTransfer [34]	1944	2.08	0.34	0.93	23.31
	Cosmos-Transfer1 [41]	1597	1.71	0.26	0.64	23.79
	<i>DreamTransfer</i>	2894	1.36	0.20	0.33	23.74
Average	RoboTransfer [34]	2298	2.85	0.39	1.30	23.94
	Cosmos-Transfer1 [41]	2097	2.01	0.27	0.71	24.61
	<i>DreamTransfer</i>	<b>3270</b>	<b>1.77</b>	<b>0.23</b>	<b>0.54</b>	<b>24.68</b>

then perform post-training using the corresponding task-specific data. To ensure a fair comparison, all experiments for a given task are trained under the same configuration. More detailed training configurations are provided in Appendix C.2.

Traditional robot policy learning evaluation focuses on task success rate, but this binary indicator often cannot fully reflect the performance of the policy. To address this, we formulate a behavioral scoring system for each task to assess intermediate progress and execution quality. Specifically, we decompose each task into several critical stages. One point is awarded for the successful completion of each stage. To ensure comparability, we normalize these scores to  $[0, 5]$ . The detailed scoring rules are provided in Appendix C.3.

Across all tasks, the visual appearances of the foreground objects in the evaluation environments are entirely distinct from those in the collected real data. Each reported result is averaged over 10 trials and 4 distinct foreground objects with **zero-shot** appearances, resulting in 40 evaluation trials per setting.

**Experimental platform.** Experiments run on an Agilix CobotMagic platform with two PiPER arms and three Intel RealSense D435i cameras (two wrist-mounted, one head-mounted).

#### 4.2.1. Comparison with Baseline Generation Models and Generalization Tests.

As shown in Table 2, among the first three rows under each VLA, different video generation models lead to significant performance gaps in downstream VLA policies for real-world robotic tasks.

Training without data augmentation yields the lowest

performance across all tasks, highlighting the necessity of generated data for policy generalization under novel visual conditions. Policies trained with data augmented by Cosmos-Transfer1 [41] show moderate improvements over the no-augmentation baseline. This is particularly evident in success rate but performance still falls short in handling complex deformable object manipulation, as shown by the relatively low success rate on `Fold Clothes`. In contrast, *DreamTransfer* achieves consistent and substantial improvements across all three tasks, outperforming both the no-augmentation baseline and Cosmos-Transfer1 [41] in both behavior score and success rate. Notably, on `Fold Clothes`, *DreamTransfer* achieves 65% and 75% success rates under  $\pi_0$  and  $\pi_{0.5}$  respectively, nearly doubling the success rate of the non-augmented baseline. This demonstrates that multi-view consistent, geometrically plausible video generation enables more effective policy learning, especially for challenging tasks involving non-rigid dynamics.

#### 4.2.2. Impact of generated data mixing ratio on real-world robot performance.

We study how the mixing ratio between real and generated data affects policy performance, while keeping the total amount of training data and the number of training steps fixed across all mixing ratios for a given task. During training, each training sample is drawn from  $D_G$  with probability  $\alpha$  and from  $D_R$  otherwise, where  $\alpha$  serves as the data mixing ratio [52].

As shown in Figure 4, performance improves significantly when generated data is introduced, peaking at a 50% mixing ratio. This balanced mix achieves optimal generalization, particularly on appearance-sensitive tasks

Table 2. Comprehensive real-world robot task performance comparison across video generation models, and training strategies. No.Aug. denotes training on real data only. † denotes that the generated data in the training set are used without applying the video quality filter. Both FixMix and *AdaMix* employ a video quality filter before training. FixMix uses uniform sampling with constant weights during training. Score is the behavior score; SR is success rate. Results are averaged over 10 trials across 4 distinct visual variations of the foreground object. Best results are in **bold**.

VLA	Method	Fold Clothes		Clean Desk		Throw Bottle		Average	
		Score	SR	Score	SR	Score	SR	Score	SR
$\pi_0$ [3]	No.Aug.	3	10%	4.1	67.5%	2.1	12.5%	3.1	30%
	Cosmos-Transfer1† [41]	3.3	40%	4	70%	3.2	40%	3.5	50%
	<i>DreamTransfer</i> †	4.4	65%	4.4	77.5%	3.2	52.5%	4	65%
	<i>DreamTransfer</i> +FixMix	4.4	70%	4.5	77.5%	3.6	57.5%	4.2	68.3%
	<i>DreamTransfer</i> + <i>AdaMix</i>	<b>4.6</b>	<b>77.5%</b>	<b>4.7</b>	<b>90%</b>	<b>4.4</b>	<b>70%</b>	<b>4.6</b>	<b>79.2%</b>
$\pi_{0.5}$ [20]	No.Aug.	3.4	27.5%	4.4	70%	2.7	32.5%	3.5	43.3%
	Cosmos-Transfer1† [41]	4.1	67.5%	4.6	77.5%	3.1	45%	3.9	63.3%
	<i>DreamTransfer</i> †	4.4	75%	4.7	85%	3.7	60%	4.3	73.3%
	<i>DreamTransfer</i> +FixMix	4.5	77.5%	4.6	87.5%	3.6	60%	4.2	75%
	<i>DreamTransfer</i> + <i>AdaMix</i>	<b>4.6</b>	<b>82.5%</b>	<b>4.8</b>	<b>92.5%</b>	<b>4.2</b>	<b>72.5%</b>	<b>4.5</b>	<b>82.5%</b>

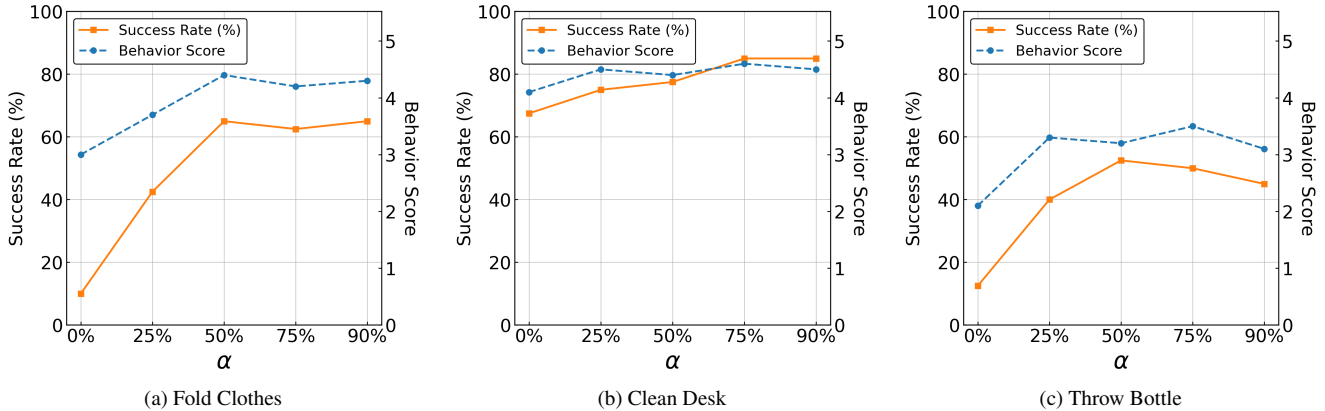


Figure 4. Impact of data mix ratios on real-world robotic tasks performance.

like Fold Clothes, where success rate jumps from 10% (real data only) to 65%. Beyond 50%, performance plateaus: increasing the proportion of generated data to 75% or 90% yields no further gain in average success rate and slightly reduces consistency. Notably, at 90% generated data, the Throw Bottle task exhibits a drop in success rate. This suggests that excessive reliance on generated data may propagate subtle visual or dynamic inaccuracies that harm performance in fast, precision-critical tasks. This result also highlights the need for the video quality filter in our *EMMA* framework to remove visually or physically unrealistic demonstrations.

#### 4.2.3. Ablation study on *AdaMix* training framework.

To evaluate the effectiveness of the *AdaMix* training strategy in improving real-world policy performance, we conduct a controlled incremental training experiment. Both methods

are trained for the same number of steps on each task, using an identical dataset comprising real data and generated data. The training process begins with the same initialization: all samples that pass the video quality filter are assigned equal initial weights, while low-quality samples are assigned zero weight and excluded from training. 8% of the Fold Clothes data and 5% each of the Clean Desk and Throw Bottle data are filtered out as low-quality. The key difference lies in whether sampling weights are adapted during training.

In the FixMix baseline, sampling weights remain constant throughout training, implementing uniform sampling over the retained data. In contrast, *AdaMix* dynamically updates the sampling weights after the first half of training steps, using trajectory performance scores to up-weight more challenging and informative samples (see Section 3.3 for details). *AdaMix* is applied jointly to both real and

Table 3. Comparison of execution time (Time, seconds), trajectory smoothness (Smth., angular acceleration in  $\text{rad}/\text{s}^2$ ) and joint overlimit (JOL., frames) between FixMix and *AdaMix* training strategies on real-world robotic tasks. Detailed calculations for these metrics are provided in Appendix C.3. Lower values are better for all metrics. Best results are in **bold**.

Method	Fold Clothes			Clean Desk			Throw Bottle			Average		
	Time	Smth.	JOL.	Time	Smth.	JOL.	Time	Smth.	JOL.	Time	Smth.	JOL.
FixMix	40.4	<b>2.2</b>	56.1	12.1	2.6	<b>60.0</b>	46.0	<b>1.2</b>	14.6	32.8	2.0	43.6
<i>AdaMix</i>	<b>39.8</b>	<b>2.2</b>	<b>53.4</b>	<b>11.3</b>	<b>2.4</b>	64.9	<b>38.9</b>	<b>1.2</b>	<b>10.4</b>	<b>30.0</b>	<b>1.9</b>	<b>42.9</b>

generated data for hard sample identification, and its key strength is being seamlessly compatible with generated and real data during training.

As summarized in Table 2, *AdaMix* consistently improves task performance across all VLA policies. Compared to FixMix, it increases the average success rate by 10.9% for  $\pi_0$  and by 7.5% for  $\pi_{0.5}$ . Beyond task completion, the policy trained with *AdaMix* demonstrates improved execution quality, as quantified in Table 3. On average, it completes tasks 2.8 seconds faster, reduces joint limit violations by 0.7 frames, and achieves slightly smoother trajectories. These improvements across all tasks, particularly in challenging scenarios like `Fold Clothes` and `Throw Bottle`, indicate that our trajectory quality metrics effectively identify difficult samples where the policy struggles.

VLA policies trained with FixMix often struggle with imprecise grasps that trigger lengthy corrective actions like re-grasping. In contrast, the improved grasp accuracy and motion stability from *AdaMix* help the policy avoid such failures, resulting in consistently more efficient task performance. Video evidence of the real-world deployment is available in the supplementary materials.

#### 4.2.4. Hyperparameter analysis of $\gamma$ and $\lambda$ .

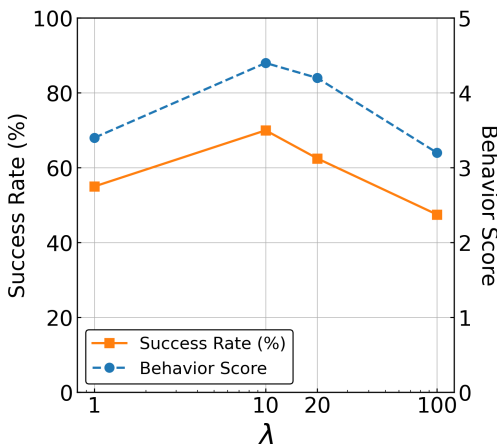


Figure 5. Performance of the policy under different  $\lambda$  with fixed  $\gamma = 1$ .

We analyze the impact of the hyperparameters  $\gamma$  and  $\lambda$  in

the sampling weight defined in Equation 7. The evaluation is conducted on the `Throw Bottle` task. We fix  $\gamma = 1$  to ensure all samples receive non-zero sampling probability and vary  $\lambda \in \{1, 10, 20, 100\}$ . The result is shown in Figure 5. When  $\lambda = 1$ , the policy performs similarly to uniform sampling, indicating insufficient focus on hard examples. Larger values of  $\lambda$  degrade performance. This suggests that over-prioritizing hard samples reduces exposure to informative easy cases and amplifies noise or outliers. These results indicate that  $\lambda = 10$  provides an effective trade-off between hard-sample focus and data diversity, while  $\gamma = 1$  ensures baseline coverage.

#### 4.2.5. Ablation study on the trajectory quality metrics.

We conduct an ablation study to evaluate the individual contribution of each metric used in computing the sample difficulty in Equation 6. The evaluation is performed on the `Throw Bottle` task. The results, summarized in Table 4, show that removing any one metric leads to a consistent decline in both success rate and behavior score, and no single metric dominates performance across all conditions. Specifically, action MSE has the strongest individual impact, but smoothness and joint angle limitation still provide complementary benefits that improve overall robustness.

Table 4. Ablation study on trajectory quality metrics. Each row shows a different metric combination for computing  $s_i$ .

Action MSE	Smoothness	Joint Limitation	Score	SR
✓	✓	✓	4.4	70%
✓	✓		4.2	62.5%
✓		✓	3.9	55%
	✓	✓	3.7	55%

### 4.3. Simulation Experiments

**Simulation setup.** We conduct simulation experiments in the RoboTwin 2.0 [9] on the `Stack Bowls Two` task. We collect 50 original demonstration trajectories, where the visual appearance of objects is consistent across different demonstrations. Using *DreamTransfer*, we generate an additional 50 demonstrations with diverse object appearances at a 1:1 ratio relative to the original data.

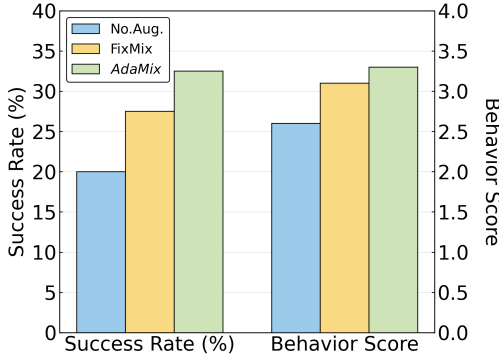


Figure 6. Task success rate and behavior score under different training data and mixing strategies in simulation experiments.

Table 5. Comparison of trajectory quality metrics between FixMix and *AdaMix* training strategies. Best results are in **bold**.

Method	Time	Smoothness	Joint Overlimit
FixMix	12.7	<b>1.9</b>	59.1
<i>AdaMix</i>	<b>12.3</b>	<b>1.9</b>	<b>43.4</b>

We consider three training settings: (i) *No.Aug.*, which uses only the original simulated demonstrations; (ii) *FixMix*, which trains on both original and generated demonstrations with uniform sampling weights after applying the video quality filter (6% of the data is filtered out); and (iii) *AdaMix*, which uses the same filtered dataset but updates sampling weights adaptively during training based on trajectory performance scores. All policies are trained using the  $\pi_0$  architecture and training configurations detailed in Appendix C.2. For evaluation, we test each policy in environments with bowls of unseen visual appearances. Each policy is evaluated over 40 trials. The behavior score rules are provided in Appendix C.3.

**Results.** As shown in Fig 6 and Table 5, training with additional data generated by *DreamTransfer* consistently improves task success rate compared with using only original demonstrations. Moreover, the proposed *AdaMix* strategy further enhances performance over the baseline mixing scheme. These observations align with our real-world robot evaluations.

## 5. Conclusion

In this paper, we address the challenge of scaling up diverse and generalizable VLA learning for robot manipulation, where real-world data collection is costly and simulation lacks realism. We present *EMMA*, a framework for enhancing VLA policy via text-guided embodied manipulation video generation with *DreamTransfer* and adaptive training with *AdaMix*. We evaluate *EMMA* on real-world robotic tasks with rigid and deformable objects under zero-shot condition. *EMMA* achieves over

a 92% improvement in success rate compared to training on real data alone, with an additional 17% gain from *AdaMix*. These results demonstrate that *EMMA* provides an effective way to enhancing the generalization of VLA.

## References

- [1] Chenxin An, Zhihui Xie, Xiaonan Li, Lei Li, Jun Zhang, Shansan Gong, Ming Zhong, Jingjing Xu, Xipeng Qiu, Mingxuan Wang, and Lingpeng Kong. Polaris: A post-training recipe for scaling reinforcement learning on advanced reasoning models, 2025. 5
- [2] Shuai Bai, Keqin Chen, Xuejing Liu, Jialin Wang, Wenbin Ge, Sibao Song, Kai Dang, Peng Wang, Shijie Wang, Jun Tang, Humen Zhong, Yuanzhi Zhu, Mingkun Yang, Zhao-hai Li, Jianqiang Wan, Pengfei Wang, Wei Ding, Zheren Fu, Yiheng Xu, Jiabo Ye, Xi Zhang, Tianbao Xie, Zesen Cheng, Hang Zhang, Zhibo Yang, Haiyang Xu, and Junyang Lin. Qwen2.5-vl technical report, 2025. 1
- [3] Kevin Black, Noah Brown, Danny Driess, Adnan Esmail, Michael Equi, Chelsea Finn, Niccolo Fusai, Lachy Groom, Karol Hausman, Brian Ichter, Szymon Jakubczak, Tim Jones, Liyiming Ke, Sergey Levine, Adrian Li-Bell, Mohith Motukuri, Suraj Nair, Karl Pertsch, Lucy Xiaoyang Shi, James Tanner, Quan Vuong, Anna Walling, Haohuan Wang, and Ury Zhilinsky.  $\pi_0$ : A vision-language-action flow model for general robot control, 2024. 2, 6, 8
- [4] Andreas Blattmann, Tim Dockhorn, Sumith Kulal, Daniel Mendelevitch, Maciej Kilian, Dominik Lorenz, Yam Levi, Zion English, Vikram Voleti, Adam Letts, Varun Jampani, and Robin Rombach. Stable video diffusion: Scaling latent video diffusion models to large datasets, 2023. 3, 6
- [5] Anthony Brohan, Noah Brown, Justice Carbajal, Yevgen Chebotar, Xi Chen, Krzysztof Choromanski, Tianli Ding, Danny Driess, Avinava Dubey, Chelsea Finn, Pete Florence, Chuyuan Fu, Montse Gonzalez Arenas, Keerthana Gopalakrishnan, Kehang Han, Karol Hausman, Alexander Herzog, Jasmine Hsu, Brian Ichter, Alex Irpan, Nikhil Joshi, Ryan Julian, Dmitry Kalashnikov, Yuheng Kuang, Isabel Leal, Lisa Lee, Tsang-Wei Edward Lee, Sergey Levine, Yao Lu, Henryk Michalewski, Igor Mordatch, Karl Pertsch, Kanishka Rao, Krista Reymann, Michael Ryoo, Grecia Salazar, Pannag Sanketi, Pierre Sermanet, Jaspier Singh, Anikait Singh, Radu Soricut, Huong Tran, Vincent Vanhoucke, Quan Vuong, Ayzaan Wahid, Stefan Welker, Paul Wohlhart, Jialin Wu, Fei Xia, Ted Xiao, Peng Xu, Sichun Xu, Tianhe Yu, and Brianna Zitkovich. Rt-2: Vision-language-action models transfer web knowledge to robotic control, 2023. 2, 3
- [6] Qingwen Bu, Jisong Cai, Li Chen, Xiuqi Cui, Yan Ding, Siyuan Feng, Xindong He, Xu Huang, et al. Agibot world colosseum: A large-scale manipulation platform for scalable and intelligent embodied systems. In *2025 IEEE/RSJ International Conference on Intelligent Robots and Systems (IROS)*. IEEE, 2025. 4, 1
- [7] Lawrence Yunliang Chen, Chenfeng Xu, Karthik Dharmarajan, Muhammad Zubair Irshad, Richard Cheng, Kurt Keutzer, Masayoshi Tomizuka, Quan Vuong, and Ken Gold-

- berg. Rovi-aug: Robot and viewpoint augmentation for cross-embodiment robot learning, 2024. 3
- [8] Sili Chen, Hengkai Guo, Shengnan Zhu, Feihu Zhang, Zilong Huang, Jiashi Feng, and Bingyi Kang. Video depth anything: Consistent depth estimation for super-long videos, 2025. 1, 3, 8
- [9] Tianxing Chen, Zanxin Chen, Baijun Chen, Zijian Cai, Yibin Liu, Zixuan Li, Qiwei Liang, Xianliang Lin, Yiheng Ge, Zhenyu Gu, Weiliang Deng, Yubin Guo, Tian Nian, Xuanbing Xie, Qiangyu Chen, Kailun Su, Tianling Xu, Guodong Liu, Mengkang Hu, Huan ang Gao, Kaixuan Wang, Zhixuan Liang, Yusen Qin, Xiaokang Yang, Ping Luo, and Yao Mu. Robotwin 2.0: A scalable data generator and benchmark with strong domain randomization for robust bimanual robotic manipulation, 2025. 9
- [10] Zoey Chen, Zhao Mandi, Homanga Bharadhwaj, Mohit Sharma, Shuran Song, Abhishek Gupta, and Vikash Kumar. Semantically controllable augmentations for generalizable robot learning, 2024. 3
- [11] Cheng Chi, Zhenjia Xu, Siyuan Feng, Eric Cousineau, Yilun Du, Benjamin Burchfiel, Russ Tedrake, and Shuran Song. Diffusion policy: Visuomotor policy learning via action diffusion, 2024. 3
- [12] Embodiment Collaboration, Abby O’Neill, Abdul Rehman, and et al. Open x-embodiment: Robotic learning datasets and rt-x models, 2025. 3
- [13] Shengliang Deng, Mi Yan, Songlin Wei, Haixin Ma, Yuxin Yang, Jiayi Chen, Zhiqi Zhang, Taoyu Yang, Xuheng Zhang, Wenhao Zhang, Heming Cui, Zhizheng Zhang, and He Wang. Graspvla: a grasping foundation model pre-trained on billion-scale synthetic action data, 2025. 2
- [14] Yu Fang, Yue Yang, Xinghao Zhu, Kaiyuan Zheng, Gedas Bertasius, Daniel Szafr, and Mingyu Ding. Rebot: Scaling robot learning with real-to-sim-to-real robotic video synthesis, 2025. 3
- [15] Haoran Geng, Feishi Wang, Songlin Wei, Yuyang Li, Bangjun Wang, Boshi An, Charlie Tianyue Cheng, Haozhe Lou, Peihao Li, Yen-Jen Wang, Yutong Liang, Dylan Goetting, Chaoyi Xu, Haozhe Chen, Yuxi Qian, Yiran Geng, Jiageng Mao, Weikang Wan, Mingtong Zhang, Jiangran Lyu, Siheng Zhao, Jiazhao Zhang, Jialiang Zhang, Chengyang Zhao, Haoran Lu, Yufei Ding, Ran Gong, Yuran Wang, Yuxuan Kuang, Ruihai Wu, Baoxiong Jia, Carlo Sferrazza, Hao Dong, Siyuan Huang, Yue Wang, Jitendra Malik, and Pieter Abbeel. Roboverse: Towards a unified platform, dataset and benchmark for scalable and generalizable robot learning, 2025. 2
- [16] Jonathan Ho and Tim Salimans. Classifier-free diffusion guidance, 2022. 3
- [17] Jonathan Ho, Ajay Jain, and Pieter Abbeel. Denoising diffusion probabilistic models, 2020. 3
- [18] Huang Huang, Fangchen Liu, Letian Fu, Tingfan Wu, Mustafa Mukadam, Jitendra Malik, Ken Goldberg, and Pieter Abbeel. Early fusion helps vision language action models generalize better, 2025. 3
- [19] Lianghua Huang, Wei Wang, Zhi-Fan Wu, Yupeng Shi, Huanzhang Dou, Chen Liang, Yutong Feng, Yu Liu, and Jingen Zhou. In-context lora for diffusion transformers, 2024. 4
- [20] Physical Intelligence, Kevin Black, Noah Brown, James Darpinian, Karan Dhabalia, Danny Driess, Adnan Esmail, Michael Equi, Chelsea Finn, Niccolo Fusai, Manuel Y. Galkner, Dibya Ghosh, Lachy Groom, Karol Hausman, Brian Ichter, Szymon Jakubczak, Tim Jones, Liyiming Ke, Devin LeBlanc, Sergey Levine, Adrian Li-Bell, Mohith Mothukuri, Suraj Nair, Karl Pertsch, Allen Z. Ren, Lucy Xiaoyang Shi, Laura Smith, Jost Tobias Springenberg, Kyle Stachowicz, James Tanner, Quan Vuong, Homer Walke, Anna Walling, Haohuan Wang, Lili Yu, and Ury Zhilinsky.  $\pi_{0.5}$ : a vision-language-action model with open-world generalization, 2025. 2, 6, 8
- [21] Joel Jang, Seonghyeon Ye, Zongyu Lin, Jiannan Xiang, Johan Bjorck, Yu Fang, Fengyuan Hu, Spencer Huang, Kaushil Kundalia, Yen-Chen Lin, Loic Magne, Ajay Mandelkar, Avnish Narayan, You Liang Tan, Guanzhi Wang, Jing Wang, Qi Wang, Yinzheng Xu, Xiaohui Zeng, Kaiyuan Zheng, Ruijie Zheng, Ming-Yu Liu, Luke Zettlemoyer, Dieter Fox, Jan Kautz, Scott Reed, Yuke Zhu, and Linxi Fan. Dreamgen: Unlocking generalization in robot learning through video world models, 2025. 4
- [22] Yuming Jiang, Siteng Huang, Shengke Xue, Yaxi Zhao, Jun Cen, Sicong Leng, Kehan Li, Jiayan Guo, Kexiang Wang, Mingxiu Chen, Fan Wang, Deli Zhao, and Xin Li. Rynnvla-001: Using human demonstrations to improve robot manipulation, 2025. 3
- [23] Shutong Jin, Lezhong Wang, Ben Temming, and Florian T. Pokorny. Physically-based lighting generation for robotic manipulation, 2025. 3
- [24] Pushkal Katara, Zhou Xian, and Katerina Fragkiadaki. Gen2sim: Scaling up robot learning in simulation with generative models, 2023. 2
- [25] Alexander Khazatsky, Karl Pertsch, Suraj Nair, and et al. Droid: A large-scale in-the-wild robot manipulation dataset, 2025. 3
- [26] Moo Jin Kim, Karl Pertsch, Siddharth Karamcheti, Ted Xiao, Ashwin Balakrishna, Suraj Nair, Rafael Rafailov, Ethan Foster, Grace Lam, Pannag Sanketi, Quan Vuong, Thomas Kollar, Benjamin Burchfiel, Russ Tedrake, Dorsa Sadigh, Sergey Levine, Percy Liang, and Chelsea Finn. Openvla: An open-source vision-language-action model, 2024. 2, 3
- [27] Diederik P Kingma and Max Welling. Auto-encoding variational bayes, 2022. 4
- [28] Weijie Kong, Qi Tian, Zijian Zhang, Rox Min, Zuozhuo Dai, Jin Zhou, Jiangfeng Xiong, Xin Li, Bo Wu, Jianwei Zhang, Kathrina Wu, Qin Lin, Junkun Yuan, Yanxin Long, Aladdin Wang, Andong Wang, Changlin Li, Duojuan Huang, Fang Yang, Hao Tan, Hongmei Wang, Jacob Song, Jiawang Bai, Jianbing Wu, Jinbao Xue, Joey Wang, Kai Wang, Mengyang Liu, Pengyu Li, Shuai Li, Weiyan Wang, Wenqing Yu, Xincheng Deng, Yang Li, Yi Chen, Yutao Cui, Yuanbo Peng, Zhentao Yu, Zhiyu He, Zhiyong Xu, Zixiang Zhou, Zunnan Xu, Yangyu Tao, Qinglin Lu, Songtao Liu, Dax Zhou, Hongfa Wang, Yong Yang, Di Wang, Yuhong Liu, Jie Jiang, and Caesar Zhong. Hunyuanvideo: A systematic framework for large video generative models, 2025. 2

- [29] Chenxuan Li, Jiaming Liu, Guanqun Wang, Xiaoqi Li, Sixiang Chen, Liang Heng, Chuyan Xiong, Jiaxin Ge, Renrui Zhang, Kaichen Zhou, and Shanghang Zhang. A self-correcting vision-language-action model for fast and slow system manipulation, 2025. 3
- [30] Xinhai Li, Jialin Li, Ziheng Zhang, Rui Zhang, Fan Jia, Tiancai Wang, Haoqiang Fan, Kuo-Kun Tseng, and Ruiping Wang. Robogsim: A real2sim2real robotic gaussian splatting simulator, 2025. 3
- [31] Zezeng Li, Alexandre Chapin, Enda Xiang, Rui Yang, Bruno Machado, Na Lei, Emmanuel Dellandrea, Di Huang, and Liming Chen. Robotic manipulation via imitation learning: Taxonomy, evolution, benchmark, and challenges, 2025. 3
- [32] Chunru Lin, Jugang Fan, Yian Wang, Zeyuan Yang, Zhehuan Chen, Lixing Fang, Tsun-Hsuan Wang, Zhou Xian, and Chuang Gan. Ubsoft: A simulation platform for robotic skill learning in unbounded soft environments. *arXiv preprint arXiv:2411.12711*, 2024. 2
- [33] Fanqi Lin, Yingdong Hu, Pingyue Sheng, Chuan Wen, Jiacheng You, and Yang Gao. Data scaling laws in imitation learning for robotic manipulation. In *The Thirteenth International Conference on Learning Representations*, 2025. 3
- [34] Liu Liu, Xiaofeng Wang, Guosheng Zhao, Keyu Li, Wenkang Qin, Jiaxiong Qiu, Zheng Zhu, Guan Huang, and Zhizhong Su. Robottransfer: Geometry-consistent video diffusion for robotic visual policy transfer, 2025. 2, 3, 4, 6, 7, 8
- [35] Haoyu Lu, Guoxing Yang, Nanyi Fei, Yuqi Huo, Zhiwu Lu, Ping Luo, and Mingyu Ding. Vdt: General-purpose video diffusion transformers via mask modeling, 2023. 3
- [36] Enhui Ma, Lijun Zhou, Tao Tang, Zhan Zhang, Dong Han, Junpeng Jiang, Kun Zhan, Peng Jia, Xianpeng Lang, Haiyang Sun, Di Lin, and Kaicheng Yu. Unleashing generalization of end-to-end autonomous driving with controllable long video generation, 2024. 5
- [37] Zhao Mandi, Homanga Bharadhwaj, Vincent Moens, Shuran Song, Aravind Rajeswaran, and Vikash Kumar. Cacti: A framework for scalable multi-task multi-scene visual imitation learning, 2023. 3
- [38] Yao Mu, Tianxing Chen, Shijia Peng, Zanxin Chen, Zeyu Gao, Yude Zou, Lunkai Lin, Zhiqiang Xie, and Ping Luo. Robotwin: Dual-arm robot benchmark with generative digital twins (early version), 2025. 2, 4, 8
- [39] NVIDIA. Isaac Sim. 6, 2
- [40] NVIDIA, :, Niket Agarwal, Arslan Ali, Maciej Bala, and et al. Cosmos world foundation model platform for physical ai, 2025. 2, 4
- [41] NVIDIA, :, Hassan Abu Alhaja, Jose Alvarez, and et al. Cosmos-transfer1: Conditional world generation with adaptive multimodal control, 2025. 2, 3, 4, 6, 7, 8
- [42] NVIDIA, :, Johan Bjorck, Fernando Castañeda, and et al. Gr00t n1: An open foundation model for generalist humanoid robots, 2025. 2
- [43] Alec Radford, Jong Wook Kim, Chris Hallacy, Aditya Ramesh, Gabriel Goh, Sandhini Agarwal, Girish Sastry, Amanda Askell, Pamela Mishkin, Jack Clark, Gretchen Krueger, and Ilya Sutskever. Learning transferable visual models from natural language supervision, 2021. 3
- [44] Colin Raffel, Noam Shazeer, Adam Roberts, Katherine Lee, Sharan Narang, Michael Matena, Yanqi Zhou, Wei Li, and Peter J. Liu. Exploring the limits of transfer learning with a unified text-to-text transformer, 2023. 4
- [45] Xuelun Shen, zhipeng cai, Wei Yin, Matthias Müller, Zijun Li, Kaixuan Wang, Xiaozhi Chen, and Cheng Wang. GIM: Learning generalizable image matcher from internet videos. In *The Twelfth International Conference on Learning Representations*, 2024. 3
- [46] Mohit Shridhar, Lucas Manuelli, and Dieter Fox. Cliport: What and where pathways for robotic manipulation, 2021. 3
- [47] Jiaming Song, Chenlin Meng, and Stefano Ermon. Denoising diffusion implicit models, 2022. 3
- [48] Eugene Teoh, Sumit Patidar, Xiao Ma, and Stephen James. Green screen augmentation enables scene generalisation in robotic manipulation, 2024. 3
- [49] Team Wan, Ang Wang, Baole Ai, Bin Wen, Chaojie Mao, Chen-Wei Xie, Di Chen, Feiwu Yu, Haiming Zhao, Jianxiao Yang, Jianyuan Zeng, Jiayu Wang, Jingfeng Zhang, Jingren Zhou, Jinkai Wang, Jixuan Chen, Kai Zhu, Kang Zhao, Keyu Yan, Lianghua Huang, Mengyang Feng, Ningyi Zhang, Pandeng Li, Pingyu Wu, Ruihang Chu, Ruili Feng, Shiwei Zhang, Siyang Sun, Tao Fang, Tianxing Wang, Tianyi Gui, Tingyu Weng, Tong Shen, Wei Lin, Wei Wang, Wei Wang, Wenmeng Zhou, Wenten Wang, Wenting Shen, Wenyuan Yu, Xianzhong Shi, Xiaoming Huang, Xin Xu, Yan Kou, Yangyu Lv, Yifei Li, Yijing Liu, Yiming Wang, Yingya Zhang, Yitong Huang, Yong Li, You Wu, Yu Liu, Yulin Pan, Yun Zheng, Yuntao Hong, Yupeng Shi, Yutong Feng, Zeyinzi Jiang, Zhen Han, Zhi-Fan Wu, and Ziyu Liu. Wan: Open and advanced large-scale video generative models, 2025. 2, 6, 8
- [50] Boyuan Wang, Xinpan Meng, Xiaofeng Wang, Zheng Zhu, Angen Ye, Yang Wang, Zhiqin Yang, Chaojun Ni, Guan Huang, and Xingang Wang. Embodiedreamer: Advancing real2sim2real transfer for policy training via embodied world modeling, 2025. 3
- [51] Jun Wang, Yuzhe Qin, Kaiming Kuang, Yigit Korkmaz, Akhilan Gurumoorthy, Hao Su, and Xiaolong Wang. Cyberdemo: Augmenting simulated human demonstration for real-world dexterous manipulation. In *2nd Workshop on Dexterous Manipulation: Design, Perception and Control (RSS)*, 2024. 3
- [52] Adam Wei, Abhinav Agarwal, Boyuan Chen, Rohan Bosworth, Nicholas Pfaff, and Russ Tedrake. Empirical analysis of sim-and-real cotraining of diffusion policies for planar pushing from pixels, 2025. 7
- [53] Julong Wei, Shanshuai Yuan, Pengfei Li, Qingda Hu, Zhongxue Gan, and Wenchao Ding. Occllama: An occupancy-language-action generative world model for autonomous driving, 2024. 3
- [54] Sizhe Yang, Wenye Yu, Jia Zeng, Jun Lv, Kerui Ren, Cewu Lu, Dahua Lin, and Jiangmiao Pang. Novel demonstration generation with gaussian splatting enables robust one-shot manipulation, 2025. 3
- [55] Xuning Yang, Clemens Eppner, Jonathan Tremblay, Dieter Fox, Stan Birchfield, and Fabio Ramos. Robot policy eval-

- uation for sim-to-real transfer: A benchmarking perspective. In *Robot Evaluation for the Real World*, 2025. 5
- [56] Zhuoyi Yang, Jiayan Teng, Wendi Zheng, Ming Ding, Shiyu Huang, Jiazheng Xu, Yuanming Yang, Wenyi Hong, Xiaohan Zhang, Guanyu Feng, Da Yin, Yuxuan Zhang, Weihang Wang, Yean Cheng, Bin Xu, Xiaotao Gu, Yuxiao Dong, and Jie Tang. Cogvideox: Text-to-video diffusion models with an expert transformer. In *The Thirteenth International Conference on Learning Representations*, 2025. 2, 3, 6, 8
- [57] Tianhe Yu, Ted Xiao, Austin Stone, Jonathan Tompson, Anthony Brohan, Su Wang, Jaspiar Singh, Clayton Tan, Dee M, Jodilyn Peralta, Brian Ichter, Karol Hausman, and Fei Xia. Scaling robot learning with semantically imagined experience, 2023. 3
- [58] Chengbo Yuan, Suraj Joshi, Shaoting Zhu, Hang Su, Hang Zhao, and Yang Gao. Roboengine: Plug-and-play robot data augmentation with semantic robot segmentation and background generation, 2025. 2
- [59] Chengbo Yuan, Rui Zhou, Mengzhen Liu, Yingdong Hu, Shengjie Wang, Li Yi, Chuan Wen, Shanghang Zhang, and Yang Gao. Motiontrans: Human vr data enable motion-level learning for robotic manipulation policies, 2025. 3
- [60] Yang Yue, Yulin Wang, Bingyi Kang, Yizeng Han, Shenzhi Wang, Shiji Song, Jiashi Feng, and Gao Huang. Deer-vla: Dynamic inference of multimodal large language models for efficient robot execution, 2024. 3
- [61] Borong Zhang, Yuhao Zhang, Jiaming Ji, Yingshan Lei, Josef Dai, Yuanpei Chen, and Yaodong Yang. Safevla: Towards safety alignment of vision-language-action model via constrained learning, 2025. 3
- [62] Lvmin Zhang, Anyi Rao, and Maneesh Agrawala. Adding conditional control to text-to-image diffusion models, 2023. 4
- [63] Guosheng Zhao, Xiaofeng Wang, Zheng Zhu, Xinze Chen, Guan Huang, Xiaoyi Bao, and Xingang Wang. Drivedreamer-2: Llm-enhanced world models for diverse driving video generation, 2024. 4
- [64] Haoyu Zhen, Qiao Sun, Hongxin Zhang, Junyan Li, Siyuan Zhou, Yilun Du, and Chuang Gan. Tesseract: Learning 4d embodied world models, 2025. 3
- [65] Zangwei Zheng, Xiangyu Peng, Tianji Yang, Chenhui Shen, Shenggui Li, Hongxin Liu, Yukun Zhou, Tianyi Li, and Yang You. Open-sora: Democratizing efficient video production for all, 2024. 2, 6
- [66] Siyuan Zhou, Yilun Du, Jiaben Chen, Yandong Li, Dit-Yan Yeung, and Chuang Gan. Robodreamer: Learning compositional world models for robot imagination, 2024. 3
- [67] Zheyu Zhuang, RUIYU WANG, Nils Ingelhart, Ville Kyrki, and Danica Kragic. Enhancing visual domain robustness in behaviour cloning via saliency-guided augmentation. In *8th Annual Conference on Robot Learning*, 2024. 3

# EMMA: Generalizing Real-World Robot Manipulation via Generative Visual Transfer

## Supplementary Material

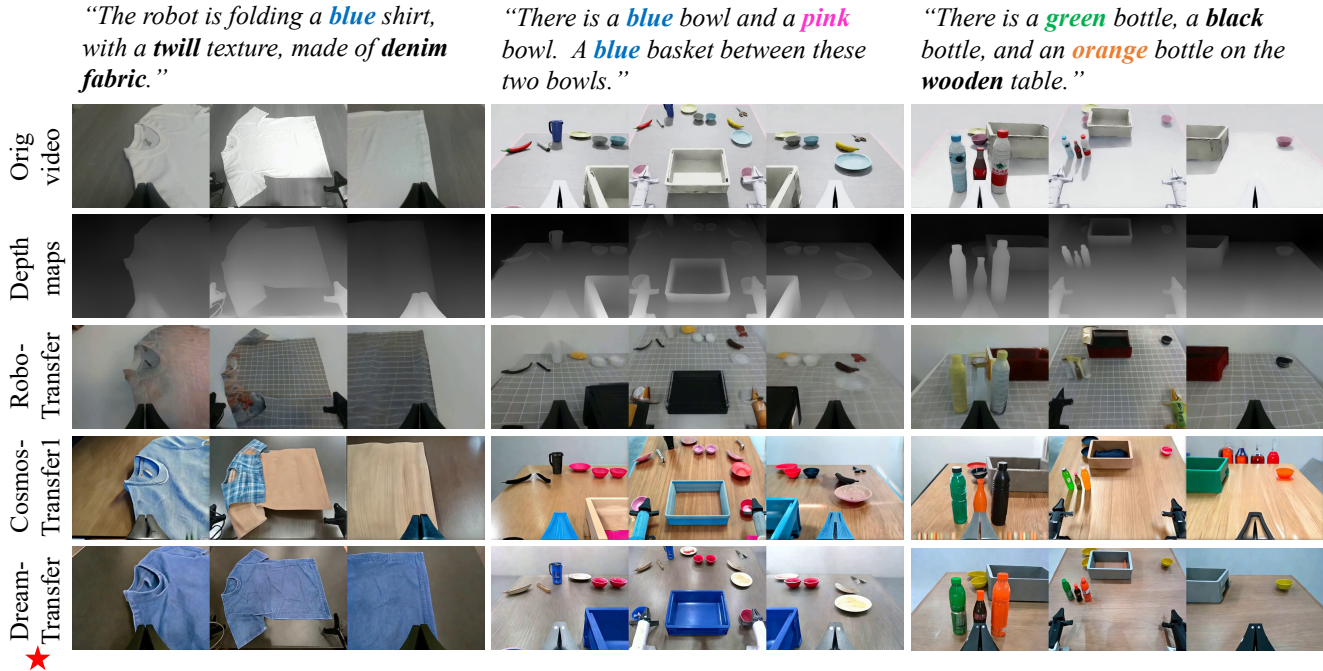


Figure 7. Qualitative comparison with state-of-the-art embodied manipulation video transfer models.

## A. Training Details of *DreamTransfer*

### A.1. Dataset Construction

To enable multi-view modeling, we construct a dataset of 50k generated multi-view video clips based on the Agibot World dataset [6], covering 36 diverse scenes. Each clip has a length of 121 frames and contains aligned multi-view RGB frames, temporally consistent depth maps, and a text caption. Depth maps are generated using the state-of-the-art estimator Video Depth Anything [8], ensuring geometric coherence across time. To support fine-grained appearance control, we utilize the prompt template shown below to structure the video captions. This template, which explicitly describes the foreground, background, and lighting conditions, is automatically populated by Qwen2.5-VL-7B-Instruct [2] to generate detailed, appearance-focused captions. One sample from the training set is illustrated in Figure 8.

#### Prompt template for video caption

##### # Task:

Please describe the robot grippers’ color, texture and material.

Do not return anything other than the appearance of the robot grippers.

##### # Example:

The robot gripper in the video is ...

The foreground of the video includes:

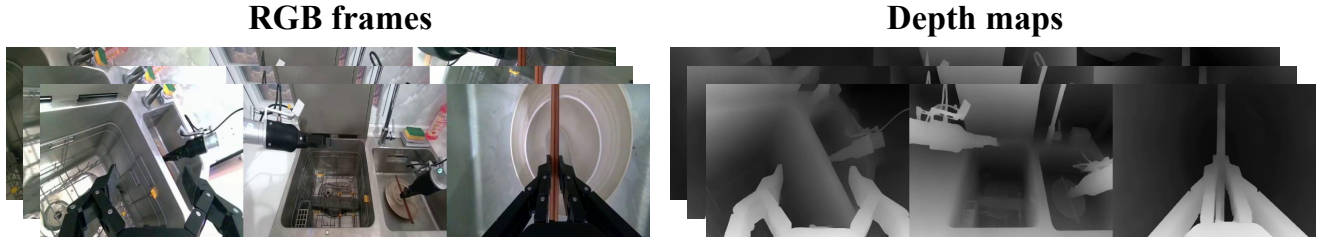
- The robot gripper is grasping ...
- The other objects are ...

The background of the video includes ...

The lighting condition in the video is ...

### A.2. Training Recipe

We designed *DreamTransfer* to perform appearance transfer directly on multi-view demonstrations from both real-



### Caption

The robot gripper in the video is black with a metallic texture and appears to be made of metal.  
 The foreground of the video includes:  
 The robot gripper is grasping a pair of chopsticks, which are brown in color, have a smooth texture, and appear to be made of wood or a similar material.  
 The other objects are a white plate and a white bowl, both located in the right sink. The plate and bowl are clean and appear to be made of ceramic or porcelain.  
 The background of the video includes:  
 1. A window with a view of trees and sky.  
 2. A stainless steel backsplash.  
 3. A bottle of dish soap on the counter.  
 4. A sponge and a scrub brush on the counter.  
 The lighting in the video is bright, with natural light coming from the window on the right side of the scene. This creates a well-lit environment that highlights the details of the kitchen sink and the objects within it. The intensity of the light is consistent across the scene, contributing to a clear and visible atmosphere.

Figure 8. Example from our multi-view embodied manipulation dataset built upon Agibot World dataset. Each sample consists of 121 aligned RGB and depth frames, along with a caption describing object and scene appearance.

Table 6. Training configurations for the two-stage training of *DreamTransfer*.

Configurations	Stage 1	Stage 2
Input Resolution (W × H)	576 × 128	1920 × 480
Batch Size	32	4
Training Steps	3500	4500
Optimizer	AdamW	AdamW
Learning Rate	$1 \times 10^{-5}$	$1 \times 10^{-5}$
Trainable Parameters	Main Branch + ControlNet	Main Branch + ControlNet
Goal	Multi-view consistency	High-res adaptation

world and simulated environments. Our real-world demonstrations are collected on the AgileX CobotMagic platform, which is equipped with three Intel RealSense D435i cameras, while the simulated demonstrations are collected in the NVIDIA Isaac Sim environment [39]. In both data sources, three synchronized cameras capture RGB images at  $640 \times 480$  resolution. We concatenate the three views along the width to form a  $1920 \times 480$  input frame for multi-view consistent modeling. Accordingly, *DreamTransfer* is trained to generate multi-view videos at  $1920 \times 480$  resolution, enabling direct multi-view video generation in one pass.

We fine-tune the pretrained Cosmos-Transfer1

model [41] on the multi-view embodied manipulation dataset detailed in Appendix A.1. However, the target resolution of  $1920 \times 480$  resolution exceeds the maximum resolution supported the pretrained Cosmos-Transfer1 model, leading to visible artifacts and noise in the generated video. To address this issue with limited computational resources, we adopt a two-stage training strategy. **Stage 1:** We stabilize the learning of multi-view geometric and appearance consistency at  $576 \times 128$  resolution. **Stage 2:** We progressively adapt the model to  $1920 \times 480$  resolution inputs while recovering high-fidelity details in out-of-distribution views. Through this two-stage training strategy, our model achieves state-of-the-art performance

with only 131 hours of training on 4 NVIDIA H20 GPUs. The detailed training configurations for each stage are summarized in Table 6.

### A.3. Computational Cost and Training Time Comparison

To ensure a fair comparison with baseline methods, we report the computational resources and training time required by each model in Table 7. All models are trained to convergence based on their respective protocols.

Table 7. Training time and computational resources for each model.

Model	Training Time	GPUs
Cosmos-Transfer1 [41]	336 hours	1024 × NVIDIA H100 GPUs
RoboTransfer [34]	96 hours	8 × NVIDIA H20 GPUs
<i>DreamTransfer</i>	131 hours	4 × NVIDIA H20 GPUs

Our two-stage training strategy enables high-quality multi-view video generation with just 131 hours of training on 4 NVIDIA H20 GPUs, requiring significantly fewer GPU hours than both RoboTransfer [34] and Cosmos-Transfer1 [41].

## B. Video Generation Quality Evaluation and Filtering Metrics

### B.1. Video Generation Quality Evaluation

To ensure the realism and fidelity of generated videos for downstream VLA policy training, we employ a set of quantitative evaluation metrics and apply corresponding filtering criteria to filter out low-quality videos. Specifically, we evaluate generated videos using five metrics: matching pixels (Mat.Pix.), root mean squared error (RMSE), absolute relative error (Abs.Rel.), squared relative error (Sq.Rel.), and CLIP similarity (CLIPSim).

**Multi-view consistency.** Consistency across camera views is quantified by the number of matching pixels between the center view and the left/right wrist-mounted views. Using a state-of-the-art image matcher [45], we compute the number of matched pixel correspondences between the center view and each side view for each frame  $t$ , denoted as  $N_{\text{match},t}^{(\text{center},\text{left})}$  and  $N_{\text{match},t}^{(\text{center},\text{right})}$ . The per-frame matching score is averaged over the two side views, and then averaged over all  $T$  frames to obtain the final Mat.Pix. score:

$$\text{Mat.Pix.} = \frac{1}{T} \sum_{t=1}^T \left[ \frac{1}{2} \left( N_{\text{match},t}^{(\text{center},\text{left})} + N_{\text{match},t}^{(\text{center},\text{right})} \right) \right]. \quad (8)$$

**Depth consistency.** To evaluate 3D structural plausibility, we extract temporally coherent depth maps from both original and generated videos using Video Depth Anything [8]. Let  $\mathbf{D}_v \in \mathbb{R}^{T \times H \times W}$  and  $\hat{\mathbf{D}}_v \in \mathbb{R}^{T \times H \times W}$  denote the ground-truth and predicted depth tensors for view

$v \in \{\text{center}, \text{left}, \text{right}\}$ , respectively. We flatten these tensors into vectors  $\mathbf{d}_v, \hat{\mathbf{d}}_v \in \mathbb{R}^N$  with  $N = THW$ , and compute the following scale-invariant error metrics:

$$\text{RMSE}_v = \frac{1}{\sqrt{N}} \left\| \hat{\mathbf{d}}_v - \mathbf{d}_v \right\|_2, \quad (9)$$

$$\text{Abs.Rel.}_v = \frac{1}{N} \sum_{n=1}^N \left| \frac{\hat{d}_{v,n} - d_{v,n}}{d_{v,n}} \right|, \quad (10)$$

$$\text{Sq.Rel.}_v = \frac{1}{N} \sum_{n=1}^N \left( \frac{\hat{d}_{v,n} - d_{v,n}}{d_{v,n}} \right)^2, \quad (11)$$

where  $d_{v,n}$  and  $\hat{d}_{v,n}$  are the  $n$ -th elements of  $\mathbf{d}_v$  and  $\hat{\mathbf{d}}_v$ , respectively. The final metric values are obtained by averaging across the three views:

$$\text{Metric} = \frac{1}{3} (\text{Metric}_{\text{center}} + \text{Metric}_{\text{left}} + \text{Metric}_{\text{right}}), \quad (12)$$

for  $\text{Metric} \in \{\text{RMSE}, \text{Abs.Rel.}, \text{Sq.Rel.}\}$ .

**Text-video alignment.** Semantic fidelity to the input prompt is measured via CLIP similarity [43]. Given a text prompt that specifies the foreground object, background scene, and lighting condition, we encode the prompt into a text embedding  $\mathbf{t}$  and compute the CLIP image embedding  $\mathbf{i}_t$  for each frame  $t$  of the center-view video. The overall CLIP similarity score is defined as the temporal average of per-frame cosine similarities:

$$\text{CLIPSim.} = \frac{1}{T} \sum_{t=1}^T \frac{\mathbf{i}_t^\top \mathbf{t}}{\|\mathbf{i}_t\| \|\mathbf{t}\|}. \quad (13)$$

### B.2. Details of the Video Quality Filter in *AdaMix*

To ensure high-quality training data for downstream vision-language-action (VLA) policy learning, we apply a strict multi-criteria filtering mechanism based on the five video quality metrics introduced in Section B.1. For each generated video, we evaluate its Mat.Pix., RMSE, Abs.Rel., Sq.Rel., and CLIP similarity scores. Only videos that simultaneously satisfy all threshold conditions specified in Table 8 are retained for training. Videos failing any single criterion are effectively excluded by setting their sampling probability to zero.

Table 8. Quality thresholds for filtering generated videos in *AdaMix*. A video is retained only if all its metric values meet the corresponding criteria.

Metric	Mat.Pix.	RMSE	Abs.Rel.	Sq.Rel.	CLIPSim.
Threshold	> 1000	< 3	< 0.4	< 1	> 20

## C. Details of Real-World and Simulated Experiments

### C.1. Tasks Setup

Figure 10 and Figure 11 shows the execution process of each task.

**Real-world experiments.** We conducted experiments on the following three real-world robot tasks, covering real-to-real and sim-to-real.

**Fold Cloth (Real-to-Real):** This is a long-horizon, multi-stage task that involves manipulating a deformable object. In the first phase, the arms cooperatively fold the cloth. In the second phase, the left arm pushes the folded cloth to a designated target location on the table.

**Clean Desk (Sim-to-Real):** In this task, a box and two bowls are placed on a tabletop. The objective is for the two robot arms to collaboratively pick up both bowls and place them inside the box.

**Throw Bottle (Sim-to-Real):** In this task, three bottles are arranged on the table, and a trash bin is positioned adjacent to it. The robot must sequentially grasp each bottle and throw it into the trash bin.

**Simulation experiments.** We conducted simulation experiments in the RoboTwin 2.0 [38] on the Stack Bowls Two.

**Stack Bowls Two:** In this task, two bowls are placed on a tabletop. The objective is for the two robot arms to collaboratively pick up both bowls and stack them at the center of the table.

### C.2. Details of Dataset and Training Configurations for VLA Policy Training

The dataset used to train the VLA policy consists of real data and generated data, with a special note for the Stack Bowls Two task: its training dataset is composed of simulated data and generated data. Real data for Fold Cloth, Clean Desk, and Throw Bottle is collected on the Agilex CobotMagic platform, while simulated data for Stack Bowls Two is collected in RoboTwin 2.0 [38] using the Aloha-AgileX embodiment. For each of these tasks, the real data is collected in a single environment with a fixed set of objects, as shown in the left column of Figure 9. For instance, the real-world data for the Fold Cloth task only contains a white shirt being folded. Generated data is synthesized using video generation models such as *DreamTransfer*, as illustrated in the right column of Figure 9. For Fold Cloth, we generate appearance-diverse data in a 1:1 manner with distinct prompts for each real data. For Clean Desk, Throw Bottle, and

Stack Bowls Two, we similarly generate appearance-diverse data in a 1:1 ratio with different prompts for each simulated data.

This setup verifies that our model can effectively leverage generated data to improve the appearance generalization ability of the VLA policy. The number of real/simulated and generated samples for each task used in VLA policy training, as well as the detailed training configurations, are summarized in Table 9. During the experiments, we found that with the same other training configuration parameters,  $\pi_{0.5}$  only requires fewer training steps to achieve performance comparable to that of  $\pi_0$ . Therefore, the number of training steps for  $\pi_{0.5}$  is set to half of that for  $\pi_0$ .

### C.3. Evaluation Details

#### C.3.1. Evaluation environment.

Figure 10 and Figure 11 show the real-world and simulated evaluation environments, respectively. In the real-world environment, the foreground objects used for evaluation have **unseen** appearances that do not appear in the training set (including real data and generated data). In the simulated environment, both the foreground objects and background exhibit **unseen** appearances that are not present in the training set (including simulated data and generated data).

#### C.3.2. Evaluation metrics details.

In real-world robot experiments, we recorded all action sequences of the robot during each task execution. Each action sequence  $a$  consists of  $T$  actions, where the action at each time step  $t$  ( $t \in \{1, 2, \dots, T\}$ ) is a  $D$ -dimensional vector, corresponding to the  $D$  joint degrees of freedom of the robot (in this study,  $D = 14$ ). We comprehensively evaluate the quality of the robot’s task execution based on five metrics: Success Rate, Behavior Score, Execution Time, Trajectory Smoothness, and Joint Overlimit.

**Success rate.** The success rate is a primary metric in traditional robot policy learning evaluation, serving as a binary indicator that reflects the proportion of successful task completions. For  $N$  independent task executions, let  $s_k$  be a binary variable where  $s_k = 1$  if the  $k$ -th execution succeeds (i.e., the task goal is fully achieved) and  $s_k = 0$  if it fails. The success rate is computed as:

$$\text{Success Rate} = \frac{1}{N} \sum_{k=1}^N s_k, \quad (14)$$

where the value ranges between 0 (all failures) and 1 (all successes). Success is defined by the robot meeting the pre-defined task objectives without critical errors.

**Behavior score.** The behavior score is a fine-grained metric that measures task progress. It provides a more nuanced evaluation than binary success/failure by allowing partial credit. Specifically, we decompose each task into several



Figure 9. Samples for training the VLA policy. The left column shows real data with fixed environments and appearances (simulated data collected from simulated environments for the `Stack Bowls Two`), while the right column shows generated data with diverse object appearances.

Table 9. The number of real/simulated and generated data for each task used in VLA policy training, as well as the detailed training configurations on each task. All pre-trained policies (e.g.,  $\pi_0$  and  $\pi_{0.5}$ ) are fine-tuned on a single task based on their open-source pre-trained weights.

Configuration	Fold Cloth	Clean Desk	Throw Bottle	Stack Bowls Two
# Real Data	50	20	20	–
# Simulated Data	–	–	–	50
# Generated Data	50	20	20	50
# Filtered Generated Data	46	19	19	47
Batch Size	64	64	64	64
Total Training Steps ( $\pi_0$ )	20000	5000	10000	1000
Total Training Steps ( $\pi_{0.5}$ )	10000	2500	5000	500
Optimizer	AdamW	AdamW	AdamW	AdamW
Warmup Steps	1000	1000	1000	1000
Init Learning Rate	$2.5 \times 10^{-8}$	$2.5 \times 10^{-8}$	$2.5 \times 10^{-8}$	$2.5 \times 10^{-8}$
Learning Rate Schedule	Cosine Decay	Cosine Decay	Cosine Decay	Cosine Decay
Trainable Parameters	All	All	All	All

critical stages. One point is awarded for the successful completion of each stage. To ensure comparability, we normalize these scores to  $[0, 5]$  using the following formula:

$$BS = \frac{N_{completed}}{N_{total}} \times 5 \quad (15)$$

where  $N_{completed}$  denotes the number of completed critical stages by the robot, and  $N_{total}$  represents the total num-

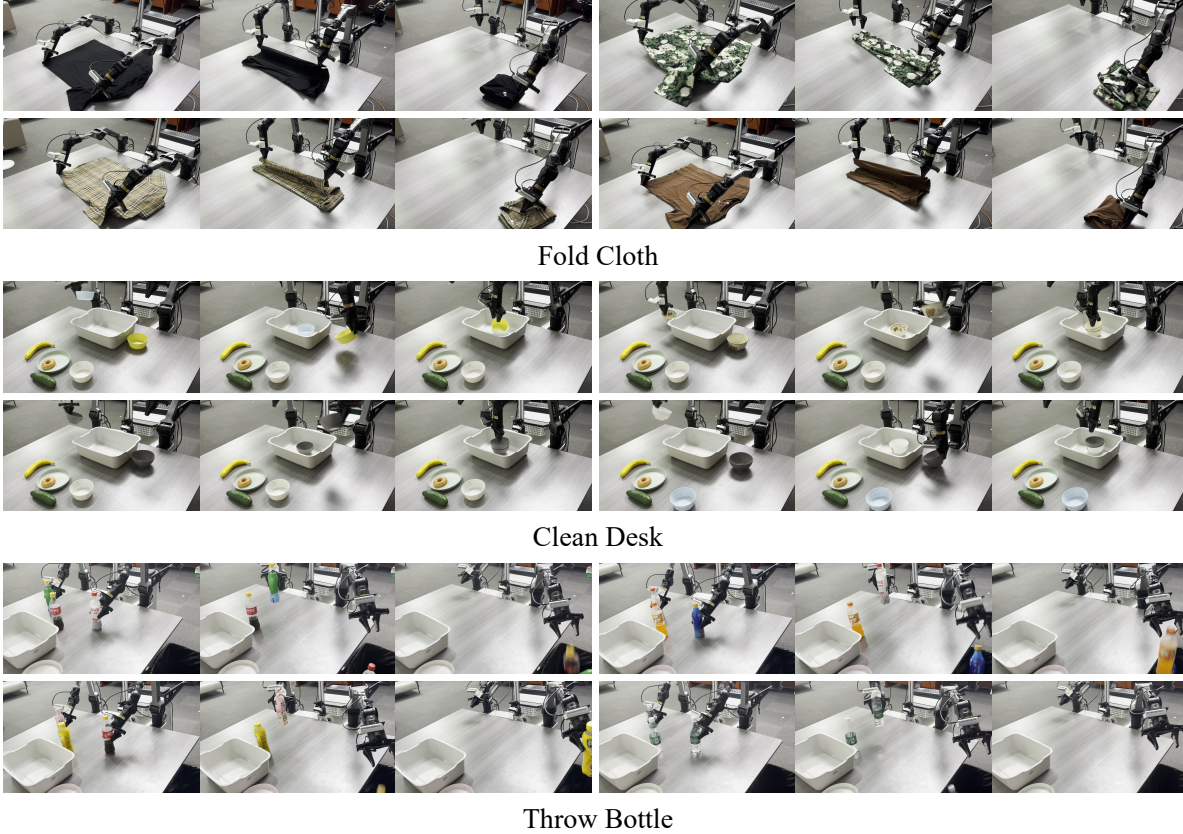


Figure 10. Real-world robot execution of  $\pi_0$  policies trained with *AdaMix* on three manipulation tasks. Full videos are provided in the supplementary material.

ber of predefined critical stages for the target task. The critical stages for each task are specified as follows:

Fold Cloth:

1. Grasp and fold the left side of the cloth.
2. Grasp and fold the right side of the cloth.
3. Grasp and fold the bottom side of the cloth.
4. Grasp and fold the top side of the cloth.
5. Push the cloth to the target position.

Clean Desk:

1. Grasp the first bowl.
2. Place the first bowl into the basket.
3. Grasp the second bowl.
4. Place the second bowl into the basket.

Throw Bottle:

1. Grasp the first bottle.
2. Throw the first bottle into the trash bin.
3. Grasp the second bottle.
4. Throw the second bottle into the trash bin.
5. Grasp the third bottle.
6. Throw the third bottle into the trash bin.

Stack Bowls Two:

1. Grasp the first bowl.
2. Place the first bowl at the center of the table.
3. Grasp the second bowl.
4. Stack the second bowl onto the first one.

**Execution time.** This metric measures the time (in seconds) taken by the robot to complete one full task. Timing starts when the robot executes its first action and ends when the task is successfully completed. To ensure reliable and fair evaluation across all trials, we define specific termination criteria for each task. For the `Fold Cloth` task, completion is defined as pushing the cloth to the target location. The `Clean Desk` task is considered complete once the second bowl is placed into the basket. Similarly, the `Throw Bottle` task concludes when the last bottle is successfully thrown into the trash bin. The `Stack Bowls Two` task is completed when the second bowl is stacked onto the first one. The average execution time is calculated only over the trials that were successfully completed.

**Trajectory smoothness.** We quantify trajectory smoothness using the mean of second-order joint angle differences,

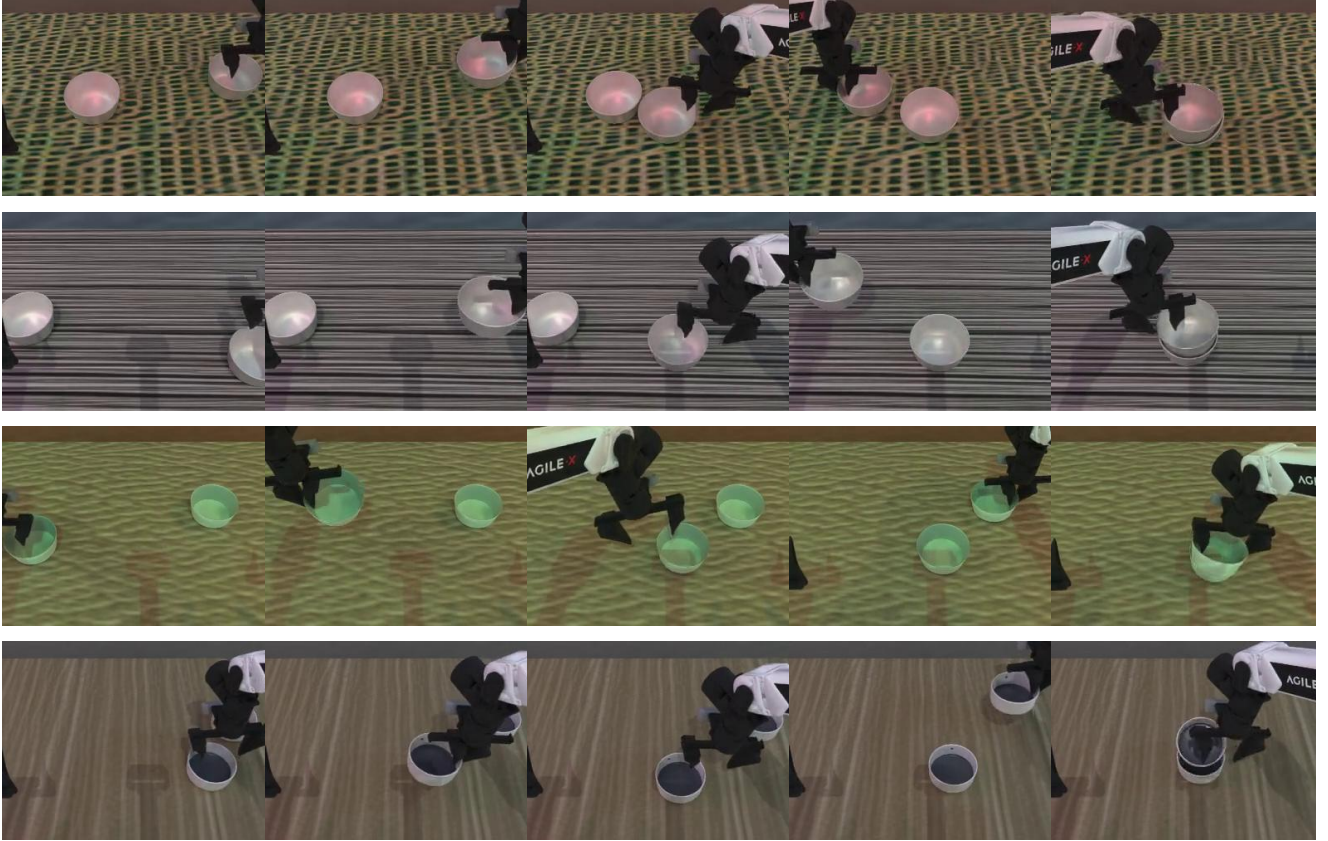


Figure 11. Simulated robot execution in RoboTwin 2.0 of  $\pi_0$  policies trained with *AdaMix* on the `Stack Bowls Two` task. Full videos are provided in the supplementary material.

defined as:

$$\text{Smoothness} = \frac{1}{D(T-2)} \sum_{i=1}^{T-2} \sum_{j=1}^D \left| \frac{\Delta^2 a_{i,j}}{(\Delta t)^2} \right|, \quad (16)$$

where  $D$  denotes the total number of joint dimensions (in this study,  $D = 14$ ),  $\Delta^2 a_{i,j} = a_{i+2,j} - 2a_{i+1,j} + a_{i,j}$  represents the second-order difference of the  $j$ -th joint angle at time step  $i$ ,  $j \in \{1, \dots, D\}$  indexes the joints,  $T$  is the total number of actions in the sequence, and  $\Delta t = 1/30$  s. The term  $T-2$  accounts for the valid range of  $i$  when computing second-order differences.

**Joint overlimit.** The Joint Overlimit metric quantifies the number of actions in the sequence where at least one joint angle exceeds its predefined limit. Formally, let  $\Omega_j = [\underline{\theta}_j, \bar{\theta}_j]$  denote the valid angle range for the  $j$ -th joint ( $j \in \{1, 2, \dots, D\}$ ), where  $\underline{\theta}_j$  and  $\bar{\theta}_j$  are the lower and upper limits of the  $j$ -th joint, respectively. For each action  $a_i = [a_{i,1}, a_{i,2}, \dots, a_{i,D}]$  at time step  $i$  ( $i \in \{1, 2, \dots, T\}$ ),

we define an indicator function:

$$\mathbb{I}(a_i) = \begin{cases} 1 & \text{if } \exists j \in \{1, 2, \dots, D\} \text{ such that } a_{i,j} \notin \Omega_j, \\ 0 & \text{otherwise.} \end{cases} \quad (17)$$

The Joint Overlimit metric is then expressed as:

$$\text{Overlimit} = \sum_{i=1}^T \mathbb{I}(a_i), \quad (18)$$

where  $T$  is the total number of actions in the sequence, and  $a_{i,j}$  represents the angle of the  $j$ -th joint in the  $i$ -th action.

## D. Qualitative Comparison with Other Video Generation Models

### D.1. Qualitative comparison.

While general video generation models exhibit strong open-domain performance, Figure 12 reveals their limitations in embodied scenarios, specifically multi-view inconsistency and poor physical fidelity. Robotic task-specialized models such as *Cosmos-Transfer1* [41] and *RoboTransfer* [34]



Figure 12. Qualitative comparison between *DreamTransfer* and general video generation models (CogVideoX [56] and Wan2.5 [49]) in embodied scenarios.

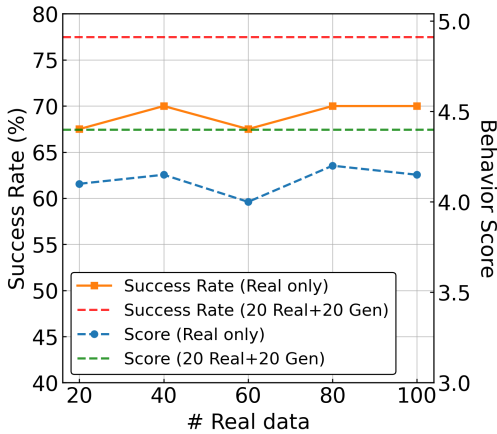


Figure 13. Evaluation of the effect of real data volume on the Clean Desk task.

leverage large-scale embodied data to achieve better kinematic plausibility, and we compare *DreamTransfer* against these specialized models.

Figure 7 presents a qualitative comparison between *DreamTransfer* and existing embodied manipulation video transfer methods [34, 41]. Our approach generates videos that maintain consistent geometry across multiple views, preserve accurate 3D structure, and respond faithfully to text-driven appearance edits, significantly outperforming prior models in visual plausibility and controllability.

Figure 14 shows diverse data generated by *DreamTransfer* from the single-appearance simulated data (first column of the last row in Figure 9) for the Stack Bowls Two task. We provide the embodied manipulation videos generated by *DreamTransfer* in the supplementary material, organized by task in the “DreamTransfer\_Generated\_Video” directory. The corresponding text prompts used for genera-

tion are available in the accompanying “prompt.json” file.

## D.2. Limitation discussion.

*DreamTransfer* generates high-quality videos with strong geometric and multi-view consistency in most scenarios. However, our depth maps are estimated from RGB videos using the Video Depth Anything [8], which may struggle in challenging cases such as fast-moving objects, large uniform-color surfaces, reflective materials, or transparent objects. Inaccurate depth estimation in these situations can lead to artifacts in the generated videos. The video quality filter in our framework effectively identifies and excludes such failed cases, preventing them from degrading the performance of the VLA policy.

## E. Qualitative Results of Policy Deployment

We evaluated the VLA policy trained with *AdaMix* in both real-world and simulated environments. In the real-world environment, we deployed the policy on the AgileX Cobot-Magic platform with two PiPER arms to execute the Fold Cloth, Clean Desk, and Throw Bottle tasks. In the RoboTwin 2.0 [38] environment, we deployed the policy on the Aloha-AgileX embodiment to perform the Stack Bowls Two task. Figure 10 and Figure 11 present the deployment results of the  $\pi_0$  policy trained with *AdaMix* in real-world and simulated environments, respectively.

These policies demonstrate the ability to generalize to real-world and simulated scenes containing objects with appearances unseen during training. Additional qualitative results are provided in the supplementary material in the “Robot\_Deployment” directory.

## F. Additional Details and Discussion

We investigate whether the performance improvements brought by *DreamTransfer* originate from a larger amount of data or from more useful and informative data. We conduct experiments on the Clean Desk task, where we additionally collect 80 real data under the same scene and object appearances. We train the  $\pi_0$  policy with 20, 40, 60, 80, and 100 real data, respectively. The training configuration follows the settings in the Clean Desk column of Table 9. Figure 13 validates that the gains arise from more useful and informative data, rather than a simple increase in data volume.

We clarify that  $\pi_0$  is adopted for the hyperparameter analysis of  $\gamma$  and  $\lambda$  in the sampling weight, as well as the ablation study on trajectory quality metrics in the Real-World Robot Evaluation section of the main paper. The training configuration follows the settings listed under the Throw Bottle column in Table 9.

*“The robot gripper is grasping bowl. Both bowls are **red**, with a **polished** texture and made of **ceramic**.”*



*“The robot gripper is grasping bowl. Both bowls are **gray**, with a **matte** texture and made of **plastic**.”*



*“The robot gripper is grasping bowl. Both bowls are **yellow**, with a **matte** texture and made of **plastic**.”*



*“The robot gripper is grasping bowl. Both bowls are **blue**, with a **smooth** texture and made of **ceramic**.”*



Figure 14. Diverse data generated by *DreamTransfer* from the simulated data (first column of the last row in Figure 9) for the `Stack BOWLS Two` task. *DreamTransfer* exhibits strong controllability in embodied manipulation video generation. Full videos and prompts are provided in the supplementary material.